

Active Sidestick Control Integration for Enhanced Aircraft Flight Envelope Protection

Çağrı Ege Altunkaya, Fatih Erol*,¹ Akın Çatak*,²
Volkan Mert***,³ Pierluigi Capone**,⁴
Şükrü Akif Ertürk***,⁵ Emre Koyuncu*,⁶

* *Istanbul Technical University, Aerospace Research Center,
Istanbul, Türkiye.*

** *Zurich University of Applied Sciences, Centre for Aviation,
Winterthur, Switzerland.*

*** *Turkish Aerospace, Air Vehicle Technologies Research Center,
Istanbul, Türkiye.*

Abstract: The design of Envelope and Pilot-Induced Oscillation (PIO) Protection Features, and Failure Cases detection and prevention using Active Control Sidestick (ACS) is a challenging task. While helping the pilot to respect the envelope limitations also in failure scenarios and, therefore, increasing mission effectiveness, these features may have a significant impact on the aircraft's agility. ACS characteristics are investigated in an integrated environment. A set of effective and flexible control laws based on Incremental Nonlinear Dynamic Inversion have been developed in a state-of-the-art aircraft simulation model and coupled with a two-ways communication with the selected ACS. The model can run in real-time in a fixed-based simulator composed of representative cockpit and out-of-the-window.

Keywords: Active Sidestick, Flight Envelope Protection, Pilot-Induced Oscillation Protection, Incremental Nonlinear Dynamic Inversion, Integrated Aircraft Simulation Model.

1. INTRODUCTION

High performance aircraft are often designed at the leading edge of technology where mission performance can be heavily impacted by deficiencies. Therefore, everything which is possible must be done to reduce pilot workload, especially in situations with rapidly changing flight conditions based on standards (USDoD (2004)).

In these scenarios the pilot might not be able to monitor the boundaries of the flight envelope (FE) in an effective way. This results in increased risks and disadvantage since the available flight performance may not be fully used (NATO AGARD (2000)). Aircraft limitations can be monitored by Envelope Protection (EP also called Carefree Handling) functions resulting in increased mission success due to reduced workload, more aggressive maneuvering, and reduced risk. Examples for EP functions from the literature are (Lombaerts et al. (2017)), (Simon et al. (2017)), (Yu et al. (2020)) and,(Moreira et al. (2022)).

Careful design must be applied to prevent possible disadvantages of EP such as reduced agility (Gibson and Hess (1997)). Therefore, an integrated approach to these features where the EP algorithm is coupled with an ACS (SAE (2007) and (SAE (2018))), able to change its char-

acteristics during the mission, is highly recommended (Akmenek (2018)). Similar reasoning can be made for PIO detection and prevention mechanisms. A more integrated solution will allow to cope with possible limitations of the aircraft system in specific points of FE. Additionally, possible failure conditions affecting ACS should be considered and coped with using detection and reconfiguration approaches.

The motivation of this work is to understand the ACS characteristics and to develop advanced flight protection algorithms within these scope. Therefore, an integrated framework shall be set up for further demonstrations.

The paper is organized as follows. In Section 2, the motivation of the work and the problem statement is described. Section 3 details the integrated framework setup such as simulation models and all the components of the simulation environment. The architecture of flight envelope protection is explained in Section 4. Preliminary test results and the initial outcomes are given in Section 5. Finally, the conclusions are given in Section 6.

2. PROBLEM STATEMENT

Many current high-performance aircraft are equipped with Active Control Sidesticks (ACS). However, the details

* This work has been submitted to IFAC for possible publication.

¹ 1st author (altunkaya16@itu.edu.tr; erolfa@itu.edu.tr)

² 2nd author (catak15@itu.edu.tr)

³ 3rd author (volkan.mert@tai.com.tr)

⁴ 4th author (capo@zhaw.ch)

⁵ 5th author (sukruakif.erturk@tai.com.tr)

⁶ 6th author (emre.koyuncu@itu.edu.tr)

of these applications are often not publicly accessible. The design of Envelope Protection (EP), Pilot-Induced Oscillation (PIO) protection, and failure case detection and prevention using ACS is a challenging task. These features help pilots adhere to envelope limitations even in failure scenarios, thereby increasing mission effectiveness. However, they can also significantly impact the aircraft's agility. A thorough understanding of these issues is crucial for designing current and future aircraft more effectively and efficiently.

To address these challenges, several key research questions must be answered: What integrated infrastructure is needed to develop and test EP and PIO prevention algorithms? Which existing EP and PIO prevention algorithms are the most effective? What are the advantages and disadvantages of ACS? What are the likely failure scenarios of an ACS, and how can they be mitigated?

The proposed research aims to address these questions through a focus on five main areas: i) building understanding of ACS features and mathematical models, ii) integrating flight envelope protection (FEP), PIO detection and prevention algorithms, and iii) demonstration. This paper details the development of an integrated framework designed to answer these research questions and presents preliminary test results.

The framework comprises several key elements: the aircraft simulation model, flight control laws, active control sidestick, visual system, and cockpit. The aircraft simulation model is designed to be representative of modern high-performance aircraft, capable of running in real-time, interfacing with all other components, supporting detailed linear and non-linear analyses, and collecting and saving all simulation data. Flight control laws must be representative of current protection algorithms as benchmarks and should support advanced protection algorithms. The active control sidestick should incorporate state-of-the-art ACS features and enable two-way communication with the simulation model.

The visual system is required to operate in real-time with latency suitable for task evaluation and to represent dedicated mission task elements accurately. The cockpit should implement a Hands on Throttle and Stick (HOTAS) system and support touch-screen instrument panels. By integrating these components, the framework aims to address the challenges in designing effective EP and PIO protection features, thus enhancing the safety and performance of high-performance aircraft.

This integrated approach ensures a comprehensive understanding of ACS characteristics and the development of advanced flight protection algorithms, ultimately contributing to more efficient and safer aircraft designs.

3. INTEGRATED ACTIVE SIDESTICK CONTROL SYSTEM

3.1 Aircraft Model

In this section, the backbone dynamic, which is a generic F-16 model, are briefly presented, and these equations establish the foundation for the nonlinear flight dynamics

model. Furthermore, the aerodynamic and actuator modeling are introduced with relevant references.

Equations of Motion The rigid non-linear body dynamics is given in a compact form in Eq. (1) and Eq. (2).

$$\dot{\mathbf{V}} = m^{-1}[\mathbf{F} - \boldsymbol{\omega} \times m\mathbf{V}] \quad (1)$$

$$\dot{\boldsymbol{\omega}} = J^{-1}[\mathbf{M} - \boldsymbol{\omega} \times J\boldsymbol{\omega}] \quad (2)$$

where $\mathbf{V} \in \mathbb{R}^{3 \times 1}$ is the body velocity vector, $\boldsymbol{\omega} \in \mathbb{R}^{3 \times 1}$ is the angular rate vector, $\mathbf{F} \in \mathbb{R}^{3 \times 1}$ is the total body force vector, $\mathbf{M} \in \mathbb{R}^{3 \times 1}$ is the total moment vector, $J \in \mathbb{R}^{3 \times 3}$ is the inertia tensor, and m is the mass of the aircraft. Additionally, the rotational kinematics are given by Eq. (3).

$$\dot{\boldsymbol{\Omega}} = \begin{bmatrix} 1 & \sin \phi \tan \theta & \cos \phi \tan \theta \\ 0 & \cos \phi & -\sin \phi \\ 0 & \sin \phi \sec \theta & \cos \phi \sec \theta \end{bmatrix} \boldsymbol{\omega} \quad (3)$$

where $\boldsymbol{\Omega}$ denotes the Euler angles.

Aerodynamics Aerodynamic modeling is constructed using the data provided in Nguyen (1979), which consists of wind tunnel test data conducted up to 0.6 Mach. All the data provided are implemented into interpolation lookup tables. After interpolation, the force and moment coefficients are calculated according to the formulation given in the same document Nguyen (1979), and dimensionalization is carried out using the necessary atmospheric and geometric properties.

Actuators The dynamics of actuators are treated as a first-order system with the time-constant, rate, and position saturation constraints, as specified in Nguyen (1979). Each control surface has a time constant of 0.0495s (that gives circa 20 rad/s), whereas rate saturations are 60°/s, 80°/s, and 120°/s for the horizontal tail, ailerons, and rudder respectively. Moreover, the position saturation are ±25°, ±21.5°, and ±30° for the horizontal tail, aileron, and rudder, respectively.

3.2 Flight Control

The control augmentation system consists of a single-loop angular rate control law using the incremental nonlinear dynamic inversion (INDI). The derivation of the control law is quite straightforward due to the control-affine form of Euler's equations of motion, given by Eq. (4) in a decomposed form.

$$\dot{\boldsymbol{\omega}} = -J^{-1}(\boldsymbol{\omega} \times J\boldsymbol{\omega}) + \underbrace{J^{-1}\bar{q}_\infty S \begin{bmatrix} b \\ \bar{c} \\ b \end{bmatrix}}_{g(\mathbf{x})} \Phi \underbrace{\boldsymbol{\delta}}_u \quad (4)$$

where \bar{q}_∞ , S , b , and \bar{c} are the dynamic pressure, wing area, wing span, and mean aerodynamic chord, respectively. Additionally, $\Phi \in \mathbb{R}^{3 \times n}$ represents the control effectiveness matrix, which consists of the moment coefficient derivatives with respect to control surface deflections at the current instant, with n denoting the number of control surfaces. The INDI control law for the control of the angular rates

is derived in the form given in Eq. (5) (for further details, please see Ludeña Cervantes et al. (2020)),

$$\mathbf{u} = \mathbf{g}(\mathbf{x}_0)^{-1}[\dot{\boldsymbol{\omega}}_c - \dot{\boldsymbol{\omega}}_0] + \mathbf{u}_0 \quad (5)$$

where the subscript "0" denotes the current state and $\dot{\boldsymbol{\omega}}_c \in \mathbb{R}^3$ is the virtual input to be designed, the finalized form of the control law is given in Eq. (6).

$$\boldsymbol{\delta} = \left\{ J^{-1} \bar{q}_\infty S \begin{bmatrix} b \\ \bar{c} \\ b \end{bmatrix} \Phi \right\}^{-1} [\dot{\boldsymbol{\omega}}_c - \dot{\boldsymbol{\omega}}_0] + \boldsymbol{\delta}_0 \quad (6)$$

where $\boldsymbol{\delta} \in \mathbb{R}^3$ signifies the control surface deflections, i.e. horizontal tail, aileron, and rudder, respectively. Moreover, since there are also three control surfaces ($n = 3$), the control effectivity matrix is a square matrix, that is, it is invertible unless it is rank deficient. Furthermore, the virtual input $\dot{\boldsymbol{\omega}}_c$ is provided by Eq. (7).

$$\dot{\boldsymbol{\omega}}_c = \begin{bmatrix} K_p & & \\ & K_q & \\ & & K_r \end{bmatrix} \begin{bmatrix} p_c - p \\ q_c - q \\ r_c - r \end{bmatrix} \quad (7)$$

where K_p , K_q , and K_r represent the gains for the roll, pitch, and yaw channels, respectively. The expressions presented provide the required generation of control surface deflections with respect to the pilot inputs of p_c , q_c , and r_c .

Consequently, the aforementioned relations complete the flight control law for the angular rates. The constructed flight control architecture is straightforward and flexible, allowing for seamless integration with other components and subsystems, e.g. it can accommodate various flight envelope protection algorithms and active sidestick features, facilitating the realization of a comprehensive pilot-in-the-loop environment.

3.3 Active Sidestick Control

This section explains the characterization of the active side-stick control system, which plays a crucial role in improving pilot-aircraft interactions and enabling flight envelope protection features.

STIRLING DYNAMICS[®] Compact Stick Active Inceptor is a state-of-the-art low-force development ACS and uses a mass-spring-damper model with adjustable parameters. The Inceptor Control Module (ICM) is an integrated microcomputer and brushless DC motor drive designed to be used as a common control module for a variety of compatible active control inceptors. The ICM runs the control law for the force feedback system and interfaces with the host computer in the simulator system.

The ACS grip has four switches: S1 (left), S2 (right), S3 (trim), and S4 (trigger). The default power-up mode is Disabled Mode. After the Initial Built-In Test (IBIT), the system zeroes force measurements. In Enabled Mode, the system can be commanded to provide artificial force feedback. In Jammed Mode, the motors can be commanded to lock the motion of the stick. Message transmission via UDP on Ethernet occurs only with command changes at 0-200 Hz for all axes. ACS features are sent through ID1-12s & 50 and read over ID20-24s as identification number, (ID) messages.

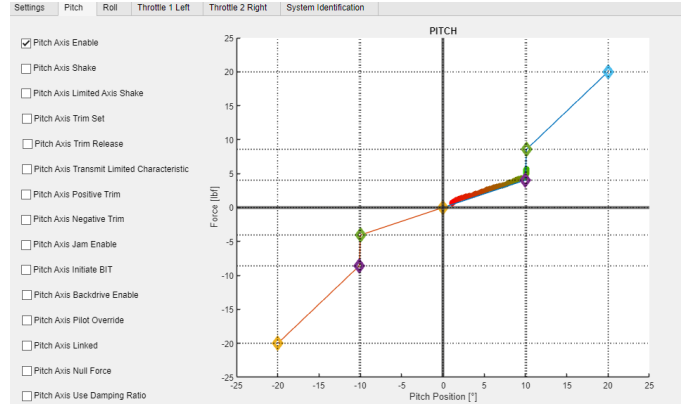


Fig. 1. Force Feel Characteristics Curve and Enable Flags

Control message (ID2) manages features including trim, shaker, and damping coefficients. The Force Feel Characteristics Curve (FFC) requires increasing force/position values. Characteristic Control (ID5) sets up the fade time when transitioning between different FFC. Trim Control (ID6) adjusts axis trim positions. Shaker Control (ID7) specifies shaker amplitude and frequency. Damping Control (ID8) sets the damping ratio (0.2-6). Cueing Force Control (ID9) adjusts cueing force characteristics. Inertia Control (ID10) defines perceived inertia (0.01-10 lbf/in²). Two ACS units can be linked for two-pilots configuration.

Rotary Status Message (ID20) reads axes status at set rates, including mode and grip switch states. Limited Characteristic Message (ID22), 'limited,' restricts control characteristics due to motor capabilities. IP Address Change (ID50) modifies network addresses.

Both pitch and roll axes have 24° position and a 27 lbf force limits, as this is a Low Force ACS. An example pitch axis configuration is shown in Fig.1.

The system's dynamics are modeled through a second-order transfer function with parameters including FFC, Damping Ratio, Moment of Inertia (MOI), and friction. The governing equation of motion is

$$m\ddot{\theta} + c\dot{\theta} = F_{char} + F_{friction} + F_{grip} \quad (8)$$

where m denotes the MOI adjusted by 0.01, and c is calculated from the damping ratio ζ and force gradient k . Assuming no friction and fixed k , the model simulates the sidestick's response to grip force $F_{grip}(s)$.

$$\theta(s) = \frac{1}{ms^2 + (2\zeta\sqrt{mk})s + k} \mathbf{F}_{grip}(s) \quad (9)$$

where $m = 0.6$, $\zeta = 0.35$, $k = 2$ and $F_{grip} = 11lbf$.

Although the ACS is similar to a mass-spring-damper system, it is a combined system with complex electrical and magnetic features. A set of different fitting methods have been used to investigate this highly nonlinear behaviour. First, the stick was moved to the deflection of 10° and then released. The recorded data was fitted with a 2nd order transfer function with 4 different approaches. Noise and system nonlinearity cause discrepancies between optimized and calculated damping and frequency values, indicating practical deviations from the theoretical model as illustrated in Fig. 2.

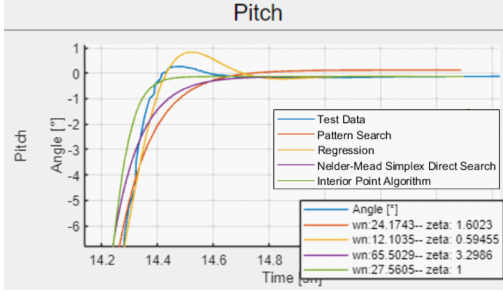


Fig. 2. The ACS Parameter Identification

4. FLIGHT ENVELOPE PROTECTION

To integrate with the ASC, a couple of conventional FEP algorithms are developed and implemented. The protection algorithms for angular rates, angle of attack, and bank angle are developed based on a common and simple rationale: applying a counter-action as a restorative measure to prevent FEP violations.

Pitch, Roll, and Yaw Rate Protection Since the commanded pilot inputs are also the angular rates, it is simply possible to restrict the pilot commands with a dynamic saturation, which is fed by the scheduled flight envelope database, to prevent a possible excess of the flight envelope. Subsequent to subjecting the pilot commands of ω_p to the maximum and minimum allowable values of the flight envelope, the resulting commanded angular rates of ω_c are then applied to the control augmentation system.

Angle of Attack and Load Factor Protection The violation of the angle of attack and load factor boundaries can be avoided by applying a 'restorative' pitch rate command. Prior to reaching the predetermined limits of the angle of attack and load factor, the pilot commands are faded out in order to prevent the aircraft from entering into an upset condition. Furthermore, both the angle of attack and load factor protection should be considered holistically to generate a single and unified restorative pitch action; therefore, the load factor boundary is also converted to the angle of attack as given by Eq. (10).

$$\alpha_{max}^{nz} = \frac{W n_{z_{max}}}{\bar{q}_{\infty} S C_{z_{\alpha}}} \quad (10)$$

where α_{max}^{nz} denotes the angle of attack equivalent to the maximum allowable load factor $n_{z_{max}}$, W is the weight of the aircraft, $C_{z_{\alpha}}$ is the force coefficient in z -direction derivative with the angle of attack. Afterward, the minimum of the main angle of attack limits, α_{max}^{α} , and equivalent angle of attack limit, α_{max}^{nz} , is used to generate the restorative action. The general framework is depicted in Fig. 3

S-I is the pitch rate protection component, which has been discussed in the preceding section. S-II is the logic of the selection of the restrictive angle of attack; furthermore, the S-III and IV consist of designed restorative actions. To ensure the generality of the generated action in terms of magnitude, normalization is performed in S-II. The normalized angle of attack indicator, $\bar{\alpha}$, reflects the current α as the percentage of α_{max}^{α} . This normalization enables the generation of a restorative pitch rate based on the

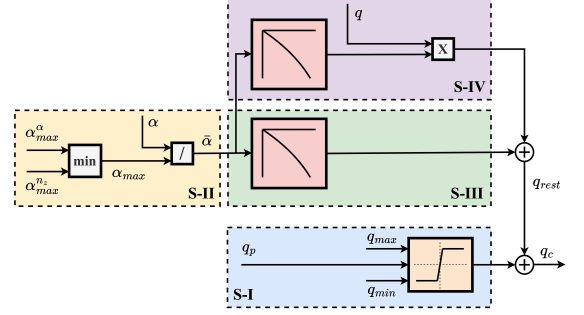


Fig. 3. The angle of attack and load factor protection scheme: four main components, S-I/II/III/IV.

proximity to the limit. Consequently, in S-IV, a damping component is incorporated to reduce the magnitude of oscillation during protection, leveraging the current pitch rate, q . Note that this structure is highly adaptable for design, and a reverse rationale can be applied to protect against violations of the minimum angle of attack and load factor limits as well.

Bank Angle Protection The bank angle protection is established with the same philosophy as the previous section. Simply, a restorative roll action is applied to not exceed the predetermined maximum allowable bank angle limit. The general framework is illustrated in Fig. 4.

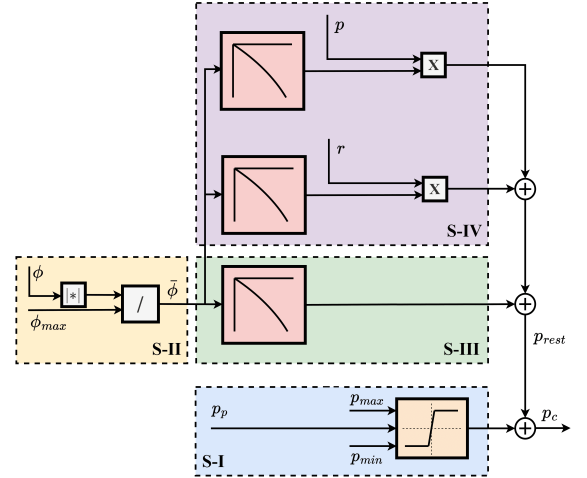


Fig. 4. The bank angle protection scheme: four main components, S-I/II/III/IV.

S-I is the roll rate protection component, while S-II is the normalization component considering the absolute of the current bank angle, ϕ . Moreover, the S-III and IV, again, consists of designed restorative actions. In S-III, a counter-action roll rate is generated based on the current bank angle as the percentage of the allowable limit. In addition, in S-IV, two distinct damping components are incorporated to fade the magnitude of oscillation out during protection, using both the current roll rate, p , and the yaw rate, r . However, the S-IV component not only addresses the roll motion-induced bank angle build-up but also accounts for the possibility of yaw motion-induced bank angle build-up. Therefore, measures are taken to protect the bank angle envelope in both scenarios.

5. SIMULATION SETUP AND RESULTS

The Visualization System runs in UNITY[®] which is a cross-platform game engine developed by Unity Technologies[™] that is primarily used to develop video games and simulations for computers, consoles, and mobile devices. The F-16 3D model has been drawn in BLENDER[®] in Fig. 5. All control surfaces have been individually separated and rigged with bones to enable independent rotation.



Fig. 5. F-16 3D CAD Model used in the Simulation Environment and Terrain Map Model in UNITY[®]

Istanbul is selected for terrain map and Istanbul Technical University is selected for reference axes. Marmara region digital elevation data is used for recreating terrain in UNITY[®] as illustrated in Fig. 5. Terrain information from Digital Terrain Elevation Data (DTED) contains only point clouds. Triangle meshes are created between these point clouds for visualization.

5.1 Aircraft Simulator Setup

The aircraft cockpit shell is equipped with an 8x20 touch screen large area display (LAD) as instrument panel, a tablet used as control panel, and a THRUSTMASTER[®] Hotas Wartog Hands-on-Throttle-and-Stick (HOTAS) system, which includes a sidestick, a dual rotary throttle, and two pedals. The general view of the integrated simulation environment is shown in Fig. 6.



Fig. 6. General view of Simulator Setup

5.2 ACS Component Interfaces

For system identification purpose of ACS, input and output signals were decoded, and tested using a network packet analyzer software that captures, aggregates, and reads data packets between local and target devices, such as Ethernet networks or recorded files as in Fig. 7. The preliminary phase also involved comprehensive diagnostics on the Low Force Inceptor, utilizing STIRLING

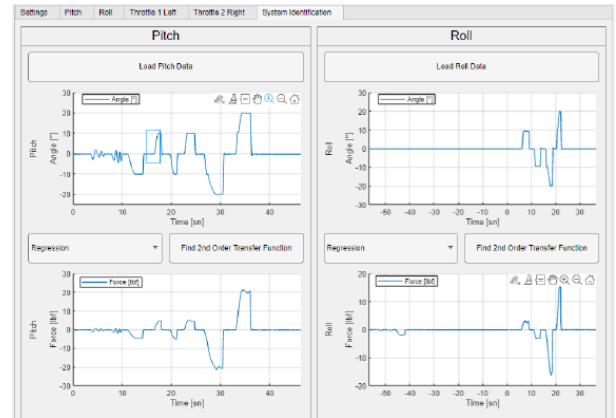


Fig. 7. Example Signal Acquisition for System Identification (pitch & roll sweeps)

DYNAMICS[®], IBIT software to confirm system integrity and operational safety.

A key aspect of the testing was the load calibration, which achieved a precision level of %2 as shown in Fig. 8. This was conducted using a load cell positioned at the detent button, facilitating accurate force measurements across control positions. Additionally, the control stick's response was evaluated from a constrained negative, down-leftmost position to a positive, upright-most position, emphasizing the robustness of the high force feedback mechanism.

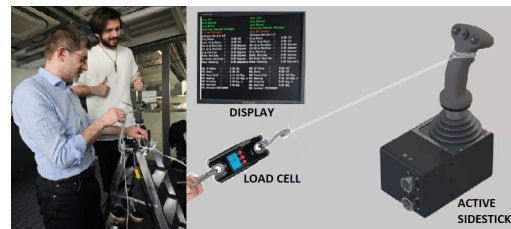


Fig. 8. Calibration Tests with Load Cell Setup

Ad hoc tests were instrumental in pinpointing uncertainties, thereby establishing definitive operational parameters, including minimum and maximum force limits and positional thresholds.

The aforementioned tests not only demonstrated the reliability of the ACS control but also revealed the identification of the axes through the binary analysis of the message header bits. This allowed for the verification of any bits that may have been overlooked between the pitch and roll axis readings. The observed discrepancies led to the implementation of alternative methodologies in subsequent development stages.

Latency was evaluated by monitoring UDP messages with scripts, which indicated a comparative decrease in efficiency against SIMULINK[®] Real-Time Blocks. Thus, it is observed that the SIMULINK[®] Real-Time Blocks are working faster. The integration of 'Matlab Functions' within SIMULINK[®] was also used to improve performance.

The commanded angular rates and their responses with respect to time are shown in Fig. 9. The performance of the flight control law is satisfactory in both decoupled and

coupled pilot inputs. The affect of envelope annihilation and the effect of flight envelope protection structure is given in Fig. 10 for longitudinal axis.

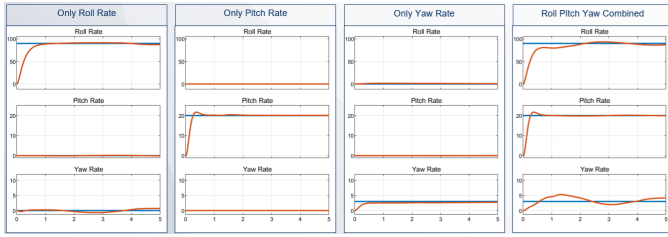


Fig. 9. Controller Outputs Integrated with Active Sidestick Control

Although the performance of the INDI controller is satisfactory it may lead to envelope exceedance if certain pitch rate command is demanded from pilot. The red lines in the Fig. 10 shows the limits in pitch, angle of attack and load factor. Even the pitch command is within the limits, it may result a in angle of attack or load factor exceedance. The results show that the proposed envelope protection algorithm prevents the exceedance before it happens.

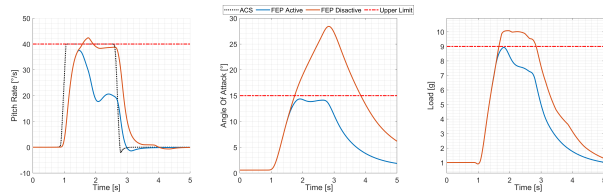


Fig. 10. Envelope Protection in Longitudinal Axis

The corresponding response of the active sidestick for the results shown in Fig.10 is given in Fig.11 to give the force displacement curve.

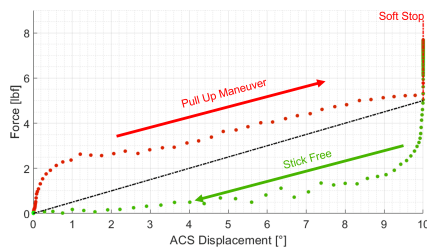


Fig. 11. ACS Displacement-Force Curve

6. CONCLUSION & OUTLOOK

This work looked on how ACS technologies can be effectively integrated in a modern Flight Control System. The focus has been on FEP functionalities and on PIO protection. Another important aspect has been to verify how ACS works with pilot inputs. This is important for making aircraft safer and more efficient. The limitations of current ACS can be identified and the corresponding pitfalls in the development of effective integrated solutions should, therefore, be avoided.

An integrated environment that takes into accounts all the different aspects and components of the problem has been built and is currently under testing. In particular, a

state-of-the-art simulation model of a high-performance aircraft has been coupled with effective and versatile control laws that will allow to develop "standard" and modern/advanced EP and PIO protection mechanisms. The model has been interfaced with 2-ways connections with a configurable ACS and also with a representative cockpit and out-of-windows.

Preliminary testing give encouraging results and confidence in the capability of the integrated framework to face the challenges of designing more easier to fly, better controllable and, ultimately, more safe aircrafts.

REFERENCES

- Akmenek, B. (2018). Testing of a flight envelope protection system for fly-by-wire aerial vehicles. *MSc thesis, Middle East Technical University.*
- Gibson, J.C. and Hess, R.A. (1997). Agard-ag-332 stick and feel system design. URL <https://www.sto.nato.int/publications/>. Last accessed 3 May 2024.
- Lombaerts, T., Looye, G., Ellerbroek, J., and Martin, M.R.y. (2017). Design and piloted simulator evaluation of adaptive safe flight envelope protection algorithm. *Journal of Guidance, Control, and Dynamics*, 40(8), 1902–1924.
- Ludeña Cervantes, T.J., Choi, S.H., and Kim, B.S. (2020). Flight control design using incremental nonlinear dynamic inversion with fixed-lag smoothing estimation. *International Journal of Aeronautical and Space Sciences*, 1–12.
- Moreira, M.A., Gripp, J.A., Yoneyama, T., and Marinho, C.M. (2022). Longitudinal flight control law design with integrated envelope protection. *Journal of Guidance, Control, and Dynamics*, 45(9), 1739–1749.
- NATO AGARD, R.W.G..S.. (2000). Rto-tr-029 flight control design - best practices. URL <https://www.sto.nato.int/>. Last accessed 3 May 2024.
- Nguyen, L.T. (1979). *Simulator study of stall/post-stall characteristics of a fighter airplane with relaxed longitudinal static stability*, volume 12854. National Aeronautics and Space Administration.
- SAE (2007). Flight control systems - general specification for design installation and test of piloted military aircraft. URL <https://www.sae.org/standards/content/as94900/>. Last accessed 3 May 2024.
- SAE (2018). Sae-arp-5764 aerospace active inceptor systems for aircraft flight and engine controls. URL <https://www.sae.org/standards/content/arp5764/>. Last accessed 3 May 2024.
- Simon, D., Härkegård, O., and Löfberg, J. (2017). Command governor approach to maneuver limiting in fighter aircraft. *Journal of Guidance, Control, and Dynamics*, 40(6), 1514–1527.
- USDoD (2004). Mil-std-1797a flying qualities of piloted aircraft. URL <https://publishers.standardstech.com>. Last accessed 3 May 2024.
- Yu, Z., Li, Y., Zhang, Z., Xu, W., and Dong, Z. (2020). Online safe flight envelope protection for icing aircraft based on reachability analysis. *International Journal of Aeronautical and Space Sciences*, 1–11.